Quadratic Regularization Design for 3D Axial CT: Towards Isotropic Noise

Jang Hwan Cho, *Member, IEEE,* and Jeffrey A. Fessler, *Fellow, IEEE*

Abstract—Potential advantages of statistical image reconstruction (SIR) methods over conventional filtered back-projection (FBP) method include reduced patient dose, improved noise and spatial resolution properties. However, the use of statistical weightings and sophisticated modeling of the system that are responsible for these improvements can lead to anisotropic and nonuniform noise characteristics and spatial resolutions. As an extension to our previous work that aimed for more isotropic and uniform spatial resolution, we propose a quadratic regularization design method for 3D axial X-ray computed tomography (CT) to achieve isotropy and uniformity of noise characteristics in the reconstructed image. In practice, noise properties may affect diagnostic quality of the reconstructed image as much as the spatial resolution. Simulations and a phantom experiment demonstrate that the proposed method leads to more isotropic and uniform noise characteristics in 3D axial CT with modest computational cost.

I. Introduction

Statistical image reconstruction methods have many potential advantages over conventional filtered back-projection (FBP) reconstruction, including improved noise and spatial resolution properties in the reconstructed image [1]. By incorporating a roughness penalty into the cost function, regularized image reconstruction methods, such as penalized weighted least squares (PWLS) methods or penalized-likelihood (PL) methods, control noise characteristics in the reconstructed image. Statistical modeling of the measurements and sophisticated system models enable such improvements in the image quality. However, their interaction with a conventional quadratic regularizer causes nonuniform and anisotropic spatial resolution and noise characteristics in the reconstructed image. Even idealized shift-invariant imaging systems suffer from this issue [2], and shift-variant modalities such as 3D axial or helical CT experience more severe problems, especially near the end slices. Several previous regularization designs aim to obtain more isotropic and uniform spatial resolution by matching the local impulse response of the estimator to a target impulse response [2]–[5]. To the best of authors knowledge, such design methods have not been applied to obtaining more desirable noise properties. In practice, noise characteristics may affect diagnostic quality of the reconstructed image as much as the spatial resolution, and obtaining more isotropic and uniform noise distribution across the entire reconstructed image can be desirable. In this paper, as an extension of [5], we

propose a regularization design for 3D axial X-ray computed tomography (CT) to improve uniformity and isotropy of noise characteristics at each voxel. Performance of the proposed method was demonstrated with simulations and a phantom experiment. The proposed method leads to more uniform and isotropic noise properties in 3D axial CT with modest computational cost.

II. Method

Consider a penalized weighted least squares (PWLS) formulation of statistical CT image reconstruction

$$\Psi(\boldsymbol{x}) = \mathsf{L}(\boldsymbol{x}) + \beta\,\mathsf{R}(\boldsymbol{x}), \quad \mathsf{L}(\boldsymbol{x}) = \frac{1}{2}\,\|\boldsymbol{y} - \boldsymbol{A}\boldsymbol{x}\|_{\boldsymbol{W}}^2, \quad (1)$$

where $\boldsymbol{x} = (x_1, \cdots, x_N)$ is the discretized version of the object being imaged, $\boldsymbol{A}$ is the system matrix, $\boldsymbol{y}$ is the measurement vector, and $\boldsymbol{W} = \mathrm{diag}\{w_i\}$ is a diagonal statistical weighting matrix whose components are inversely proportional to the measurement variances. We can express a quadratic regularizer with voxel-dependent and direction-dependent weights as:

$$\mathsf{R}(\boldsymbol{x}) = \sum_j \sum_{l=1}^{N_l} \kappa_{l(j)} \kappa_j r_j^l \frac{1}{2}\left((c_l * * * x)(n,m,z)\right)^2, \quad (2)$$

where $\{r_j^l\}$ are the directional weighting coefficients that we will design, index j is a lexicographical ordering of (n, m, z), N_l is the number of neighbors (13 in 3D), κ's are the user-defined weights that governs the spatial resolution in the reconstructed image [2], and c_l is a first-order differencing function that penalizes lth neighbor defined as

$$c_l = \frac{1}{\sqrt{n_l^2 + m_l^2 + z_l^2}}(\delta(n,m,z) - \delta(n - n_l, m - m_l, z - z_l)), \quad (3)$$

where n_l, m_l, z_l denote the offset of the neighbor.

The closed-form solution of (1) is given by

$$\hat{\boldsymbol{x}} = (\boldsymbol{H} + \beta\boldsymbol{R})^{-1}\boldsymbol{A}'\boldsymbol{W}\boldsymbol{y}, \quad (4)$$

where $\boldsymbol{H} = \boldsymbol{A}'\boldsymbol{W}\boldsymbol{A}$ and $\boldsymbol{R}$ is the Hessian of the regularizer $\mathsf{R}(\boldsymbol{x})$. If the weighting is chosen such that $\mathrm{cov}(\boldsymbol{y}) = \boldsymbol{W}^{-1}$, then the reconstruction covariance is [6]

$$\mathrm{cov}(\hat{\boldsymbol{x}}) = (\boldsymbol{H} + \beta\boldsymbol{R})^{-1}\boldsymbol{H}(\boldsymbol{H} + \beta\boldsymbol{R})^{-1}. \quad (5)$$

A. Local Power Spectrum

We assume that $\boldsymbol{A'WA\delta^j}$ and $\boldsymbol{R\delta^j}$ are approximately locally circulant [7], and approximate the local noise power spectrum of (5) near voxel j as follows:

$$S^j = \frac{F\left(\boldsymbol{A'WA\delta^j}\right)}{\left(F\left(\boldsymbol{A'WA\delta^j}\right) + \beta F\left(\boldsymbol{R\delta^j}\right)\right)^2}, \qquad (6)$$

where $F(\cdot)$ denotes the 3-D DFT and $\boldsymbol{\delta^j}$ denotes a Kronecker impulse for the jth voxel. Calculation of (6) involves two 3-D DFTs per voxel, and becomes very computationally expensive when we consider the entire image volume. Thus, we use a continuous-space analog of $H_j \triangleq F\left(\boldsymbol{A'WA\delta^j}\right)$ instead of directly using the discrete Fourier transform. In [8], H_j in spherical coordinates $\boldsymbol{\nu} \triangleq (\rho, \Phi, \Theta)$ was approximated as follows:

$$
\begin{aligned}
H_j(\boldsymbol{\nu}) &\approx KJ(\boldsymbol{\nu}) \frac{\tilde{w}_j(\Phi)}{\rho\cos(\Theta)} \qquad (7) \\
K &= \Pi\Delta_x^3\Delta_z D_{sd}^2/D_{so}^2 \\
J(\boldsymbol{\nu}) &= \mathrm{sinc}(\Delta_x\rho\cos(\Theta)\cos\Phi)^2\mathrm{sinc}(\Delta_y\rho\cos(\Theta)\sin\Phi)^2 \\
&\quad \times\mathrm{sinc}(\Delta_z\rho\sin(\Theta))^2 \\
\tilde{w}_j(\Phi) &= \sum_{\beta\in B_j(\Phi)} \frac{\bar{w}_{\beta,j}}{d_{\beta,j}\sqrt{1-(\zeta^j\cos(\theta^j))^2\cos^2(\phi^j-\Phi)}}.
\end{aligned}
$$

where K is a factor depending on voxel sizes and scanner geometry, $J(\rho, \Phi, \Theta)$ is a component depending only on spatial frequencies, $D_{so} \cdot (\zeta^j, \phi^j, \theta^j)$ denotes the location of the jth voxel in spherical coordinates, $\bar{w}_{\beta,j} \triangleq w_\beta(\bar{s}_j^*)$ where $\bar{s}_j^*$ is the positon on the detector that maximizes the footprint of voxel j at source angle β [8], $d_{\beta,j}$ is the distance from the source to the xy-projection of voxel j, and $B_j(\Phi)$ is the set of the values of β for which the ray passing through voxel j is perpendicular to the frequency vector $\boldsymbol{\nu}$ where the ray and frequency vector are both projected onto the xy-plane. See [8] for definition of each variable.

Substituting (7) into (6) leads to the following expression for the continuous space analog of the noise power spectrum S^j:

$$
\begin{aligned}
\boldsymbol{S^j} &\approx \frac{M(\boldsymbol{\nu})\tilde{w}_j(\Phi)/\rho}{\left(M(\boldsymbol{\nu})\tilde{w}_j(\Phi)/\rho + \beta R^j(\boldsymbol{\nu})\right)^2} \qquad (8) \\
M(\boldsymbol{\nu}) &= \frac{KJ(\boldsymbol{\nu})}{\cos(\Theta)},
\end{aligned}
$$

where $R^j(\boldsymbol{\nu})$ is the local frequency response of the regularizer near voxel j (see (20) below).

B. Target Local Power Spectrum

Our goal is to design the regularizer to obtain more isotropic correlation in the reconstructed image. Following [2], we approximate (5) as

$$\mathrm{cov}(\hat{\boldsymbol{x}}) \approx \left(\boldsymbol{D_\eta A'AD_\eta} + \beta\boldsymbol{R}\right)^{-1}\boldsymbol{D_\eta A'AD_\eta} \\ \times \left(\boldsymbol{D_\eta A'AD_\eta} + \beta\boldsymbol{R}\right)^{-1}, \quad (9)$$

where

$$\boldsymbol{D_\eta} = \mathrm{diag}\{\eta_j\}, \quad \eta_j \triangleq \frac{\sum_i a_{ij}^2 w_i}{\sum_i a_{ij}^2}. \qquad (10)$$

With further approximations, variance at jth voxel becomes

$$\mathrm{var}(\hat{x}_j) \approx \frac{1}{\eta_j^2}\left(\boldsymbol{A'A} + \frac{\beta}{\eta_j^2}\boldsymbol{R}\right)^{-1}\boldsymbol{A'A}\left(\boldsymbol{A'A} + \frac{\beta}{\eta_j^2}\boldsymbol{R}\right)^{-1}. \qquad (11)$$

From (11), our target, the local power spectrum at the isocenter with uniform weighting, can be written as:

$$S^0 \approx \frac{M(\boldsymbol{\nu})\tilde{u}_o(\Phi)/\rho}{\eta_o^2\left(M(\boldsymbol{\nu})\tilde{u}_o(\Phi)/\rho + (\beta/\eta_o^2)R_o(\boldsymbol{\nu})\right)^2}, \qquad (12)$$

where $\tilde{u}_o(\Phi) = |B_j(\Phi)|$, and $R_o(\boldsymbol{\nu})$ is the local frequency reponse of the regularizer at the isocenter with pre-defined directional weights, $\{r_o^l\}$, that determine the shape of the target noise power spectrum (see (21)).

We want to match the local noise power spectrum near jth voxel to the target local noise power spectrum, i.e., $S^j \approx S^0$.

$$
\begin{aligned}
S^j &\approx \frac{M(\boldsymbol{\nu})\tilde{w}_j(\Phi)/\rho}{\left(M(\boldsymbol{\nu})\tilde{w}_j(\Phi)/\rho + \beta R^j(\boldsymbol{\nu})\right)^2} \qquad (13) \\
&\approx \frac{M(\boldsymbol{\nu})\tilde{u}_0(\Phi)/\rho}{\eta_o^2\left(M(\boldsymbol{\nu})\tilde{u}_0(\Phi)/\rho + (\beta/\eta_o^2)R_o(\boldsymbol{\nu})\right)^2} \approx S^0.
\end{aligned}
$$

Cross multiplying leads to the following:

$$\tilde{u}_0(\Phi)\left(M(\boldsymbol{\nu})\tilde{w}_j(\Phi)/\rho + \beta R^j(\rho, \Phi, \Theta)\right)^2 \\ \approx \eta_o^2\tilde{w}_j(\Phi)\left(M(\boldsymbol{\nu})\tilde{u}_0(\Phi)/\rho + (\beta/\eta_o^2)R_o(\rho, \Phi, \Theta)\right)^2. \quad (14)$$

By taking the square root on both sides

$$\sqrt{\tilde{u}_0(\Phi)}\left(M(\boldsymbol{\nu})\tilde{w}_j(\Phi)/\rho + \beta R^j(\rho, \Phi, \Theta)\right) \\ \approx \eta_o\sqrt{\tilde{w}_j(\Phi)}\left(M(\boldsymbol{\nu})\tilde{u}_0(\Phi)/\rho + (\beta/\eta_o^2)R^0(\rho, \Phi, \Theta)\right). \quad (15)$$

Finally, simplifying yields

$$R^j(\rho, \Phi, \Theta) \approx \beta^{-1}\frac{M(\boldsymbol{\nu})}{\rho}\left[\eta_o\sqrt{\tilde{u}_o(\Phi)\tilde{w}_j(\Phi)} - \tilde{w}_j(\Phi)\right] \\ + \frac{1}{\eta_o}\sqrt{\frac{\tilde{w}_j(\Phi)}{\tilde{u}_o(\Phi)}}R_o(\boldsymbol{\nu}). \quad (16)$$

C. Regularization Structure

Fourier transform of (3) leads to the following expression for the local frequency response $|C_l(\omega_1, \omega_2, \omega_3)|^2$

$$
\begin{aligned}
&= \frac{1}{n_l^2 + m_l^2 + z_l^2}\left|1 - e^{-i(\omega_1 n_l + \omega_2 m_l + \omega_3 z_l)}\right|^2 \\
&= \frac{1}{n_l^2 + m_l^2 + z_l^2}\left(2 - 2\cos\left(\omega_1 n_l + \omega_2 m_l + \omega_3 z_l\right)\right). \quad (17)
\end{aligned}
$$

Using the approximation $2 - 2\cos(x) \approx x^2$ [4], (17) becomes

$$|C_l(\omega_1, \omega_2, \omega_3)|^2 \approx \frac{1}{n_l^2 + m_l^2 + z_l^2}\left(\omega_1 n_l + \omega_2 m_l + \omega_3 z_l\right)^2. \qquad (18)$$

We know the following relationship between frequency and sampling $\omega_1 = 2\pi\Delta_x\rho\cos(\Phi)\cos(\Theta)$, $\omega_2 =$

$2\pi\Delta_y\rho\sin(\Phi)\cos(\Theta)$, and $\omega_3 = 2\pi\Delta_z\rho\sin(\Theta)$. Substituting these into (18) yields the following expression for $|C_l(\omega_1,\omega_2,\omega_3)|^2$ in spherical frequency coordinates

$$\approx \frac{1}{n_l^2 + m_l^2 + z_l^2}(2\pi\rho)^2(n_l\Delta_x\cos(\Phi)\cos(\Theta)$$
$$+ m_l\Delta_y\sin(\Phi)\cos(\Theta) + z_l\Delta_z\sin(\Theta))^2 \quad (19)$$

The local frequency response of the quadratic regularizer (2) is now given as:

$$R^j(\boldsymbol{\nu}) = (2\pi\rho)^2\kappa_j\sum_{l=1}^{N_l}\kappa_{l(j)}r_l^j\left(e(\Phi,\Theta)\cdot[e(\Phi_l,\Theta_l)\otimes\Delta]\right)^2,$$
$$(20)$$

where $e(\Phi,\Theta) \triangleq (\cos(\Phi)\cos(\Theta), \sin(\Phi)\cos(\Theta), \sin(\Theta))$, $\Delta \triangleq (\Delta_x,\Delta_y,\Delta_z)$, $\otimes$ is element-wise multiplication, and we assumed that $\kappa_j \approx \kappa_l$ for l within the neighborhood of j. The target noise power spectrum, R_o now has the following expression

$$R_o(\rho,\Phi,\Theta) = (2\pi\rho)^2\kappa_0\sum_{l=1}^{N_l}\kappa_{l(0)}r_l^0\left(e(\Phi,\Theta)\cdot[e(\Phi_l,\Theta_l)\otimes\Delta]\right)^2.$$
$$(21)$$

D. Regularization Design

Substituting (20) into (16) and simplifying yields

$$Q_j(\Phi,\Theta) \approx \beta^{-1}\frac{M(\boldsymbol{\nu})}{(2\pi\rho)^2}\left[\eta_o\sqrt{\tilde{u}_o(\Phi)\tilde{w}_j(\Phi)} - \tilde{w}_j(\Phi)\right]$$
$$+ \frac{1}{\eta_o}\sqrt{\frac{\tilde{w}_j(\Phi)}{\tilde{u}_o(\Phi)}}Q_0(\Phi,\Theta), \quad (22)$$

where $Q_j(\Phi,\Theta) \triangleq \kappa_j\sum_{l=1}^{N_l}\kappa_{l(j)}r_l^j\left(e(\Phi,\Theta)\cdot[e(\Phi_l,\Theta_l)\otimes\Delta]\right)^2$. For large ρ, the second term in (22) dominates:

$$Q_j(\Phi,\Theta) \approx \frac{1}{\eta_o}\sqrt{\frac{\tilde{w}_j(\Phi)}{\tilde{u}_o(\Phi)}}Q_0(\Phi,\Theta). \quad (23)$$

We design the directional weighting coefficient vector $\boldsymbol{r}_j = (r_j^1,\cdots,r_j^{N_l})$ at the jth voxel by solving the following weighted minimization problem

$$\boldsymbol{r}^j \triangleq \arg\min_{r^j\geq 0}\int_0^{2\pi}\int_{-\frac{\pi}{2}}^{\frac{\pi}{2}}D_w(\Phi,\Theta)|\breve{w}_j(\Phi,\Theta)$$
$$- \sum_{l=1}^{N_l}r_l^j(e(\Phi,\Theta)\cdot[e(\Phi_l,\Theta_l)\otimes\Delta])^2|^2d\Theta d\Phi, \quad (24)$$

where the nonnegativity constraint ensures the regularizer's convexity and we define the modified weighting function

$$\breve{w}_j(\Phi,\Theta) \triangleq \frac{1}{\eta_o}\frac{\kappa_0^2}{\kappa_j^2}\sqrt{\frac{\tilde{w}_j(\Phi)}{\tilde{u}_o(\Phi)}}\sum_{l=1}^{N_l}r_o^l(e(\Phi,\Theta)\cdot[e(\Phi_l,\Theta_l)\otimes\Delta])^2,$$
$$(25)$$

where we assumed $\kappa_j \approx \kappa_l$ for l within the neighborhood of j. We choose $D_w = \cos(\Theta)$ so that the Riemann approximation of the integral over Θ in (25) has a more uniform effect. We sampled both Θ and Φ linearly with $\Delta\Theta = \Delta\Phi = \frac{\pi}{80}$.

The problem can be simplified using orthogonal decomposition as follows [5]. One can view (24) as a weighted projection of $\tilde{w}_j(\Phi)$ onto the space spanned by $\{[e(\Phi_l,\Theta_l)\otimes\Delta]^2\}$. After inserting the weight $\cos(\Theta)$ into the data-fitting part, we can decompose $\sum_{l=1}^{N_l}r_j^l\cos^2(\Theta)(e(\Phi,\Theta)\cdot[e(\Phi_l,\Theta_l)\otimes\Delta])^2$ as $\boldsymbol{PTr}^j$, where $\boldsymbol{P}$ is a matrix whose columns are consisting of six orthonormal vectors, and $\boldsymbol{T}$ is a $6\times N_l$ linear combination matrix whose mth row is obtained as follows

$$\boldsymbol{T}_{ml} = \frac{1}{2\pi^2}\int_0^{2\pi}\int_{-\pi/2}^{\pi/2}(e(\Phi,\Theta)\cdot[e(\Phi_l,\Theta_l)\otimes\Delta])^2p_m d\Theta d\Phi.$$
$$(26)$$

The orthonormal basis functions are given as follows

$$p_1(\Phi,\Theta) = \sqrt{\frac{8}{3}}\cos^2(\Theta)$$

$$p_2(\Phi,\Theta) = \frac{16}{\sqrt{5}}\sin(\Phi)\sin(\Theta)\cos^3(\Theta)$$

$$p_3(\Phi,\Theta) = \frac{16}{\sqrt{5}}\cos(\Phi)\sin(\Theta)\cos^3(\Theta)$$

$$p_4(\Phi,\Theta) = \sqrt{\frac{96}{5}}\cos^2(\Theta)(\cos(2\Theta) - \frac{2}{3})$$

$$p_5(\Phi,\Theta) = \frac{8}{\sqrt{35}}\cos(2\Phi)(1 + \cos(2\Theta))\cos^2(\Theta)$$

$$p_6(\Phi,\Theta) = \frac{32}{\sqrt{35}}\cos^4(\Theta)\cos(\Phi)\sin(\Phi),$$

and assuming $\Delta_x = \Delta_y$, the lth column of $\boldsymbol{T}$ is given by

$$\begin{bmatrix} \sqrt{\frac{3}{2}}(\frac{1}{4}\Delta_x^2\cos^2(\Theta_l) + \frac{1}{3}\Delta_z^2\sin^2(\Theta_l)) \\ \frac{\sqrt{5}}{5}\Delta_x\Delta_z\sin(\Phi_l)\sin(\Theta_l)\cos(\Theta_l) \\ \frac{\sqrt{5}}{5}\Delta_x\Delta_z\cos(\Phi_l)\sin(\Theta_l)\cos(\Theta_l) \\ -\frac{1}{\sqrt{30}}\Delta_z^2\sin^2(\Theta_l) \\ \frac{\sqrt{35}}{28}\Delta_x^2\cos^2(\Theta_l)(\cos^2(\Phi_l) - \sin^2(\Phi_l)) \\ \frac{\sqrt{35}}{14}\Delta_x^2\cos(\Phi_l)\sin(\Phi_l)\cos^2(\Theta_l) \end{bmatrix}.$$

The minimization problem (24) can be further simplified as

$$\boldsymbol{r}^j = \arg\min_{\boldsymbol{r}\geq 0}\left\|\boldsymbol{Tr} - \boldsymbol{b}^j\right\|^2, \quad (27)$$

where $\boldsymbol{P}^*$ denotes the adjoint of $\boldsymbol{P}$ and $\boldsymbol{b}^j \triangleq \boldsymbol{P}^*\mathring{w}_j(\cdot)$, i.e., $b_k^j = 1/(2\pi^2)\int\int p_k(\Phi,\Theta)\mathring{w}_j(\Phi,\Theta)d\Phi d\Theta$ for $k = 1,\cdots,6$, where $\mathring{w}_j(\Phi,\Theta) = \breve{w}_j(\Phi,\Theta)\cos^2(\Theta)$. (27) is a much smaller problem than (24), and can be solved easiliy using NNLS algorithm [9].

E. Additional constraints for $\boldsymbol{r}^j$

The mapping from $\boldsymbol{P}^*\mathring{w}_j$ to $\boldsymbol{r}^j$ needs to be continuous for our locally circulant approximations, so we add Tikhonov regularization to the cost function (27). Furthermore, since the minimization problem (27) is under-determined, it may have many different solutions $\boldsymbol{r}^j$ that are all global minima. We want to prevent our solution to have too many zeros because they may degrade the reconstructed image due to zeros in the Hessian [4]. We ensure that certain $\boldsymbol{r}^j$ values are greater than small positive value ϵ_l^j. Our modified NNLS problem can be

expressed as follows:

$$\boldsymbol{r}^j \quad = \quad \arg\min_{\boldsymbol{r} \geq 0} \left\| \boldsymbol{T}\boldsymbol{r} - (\boldsymbol{b}^j - \boldsymbol{T}\boldsymbol{\epsilon}^j) \right\|^2 + \tau \left\| \boldsymbol{r} \right\|^2 \quad (28)$$

$$= \quad \arg\min_{\boldsymbol{r} \geq 0} \left\| \boldsymbol{T}\boldsymbol{r} - \bar{\boldsymbol{b}}^j \right\|^2 + \tau \left\| \boldsymbol{r} \right\|^2 \quad (29)$$

$$= \quad \arg\min_{\boldsymbol{r} \geq 0} \left\| \hat{\boldsymbol{T}}\boldsymbol{r} - \hat{\boldsymbol{b}}^j \right\|^2, \quad (30)$$

where $\bar{\boldsymbol{b}}^j \triangleq \boldsymbol{b}^j - \boldsymbol{T}\boldsymbol{\epsilon}^j$, and

$$\hat{\boldsymbol{T}} = \begin{pmatrix} \boldsymbol{T} \\ \tau \boldsymbol{I} \end{pmatrix}, \quad \hat{\boldsymbol{b}} = \begin{pmatrix} \bar{\boldsymbol{b}} \\ \boldsymbol{0} \end{pmatrix}. \quad (31)$$

The value of τ should be sufficient to apply a small penalty to the norm of $\boldsymbol{r}^j$. We use the coefficients $\bar{\boldsymbol{r}}^j = \boldsymbol{r}^j + \boldsymbol{\epsilon}^j$ for our new regularizer. Due to under-determined nature of the problem and limited degrees of freedom, having other constraints may also be helpful for our solutions.

III. RESULTS

A water cylinder phantom was used to evaluate the proposed method and was scanned with a 32-slice scanner in full scan mode. The reconstruction field-of-view (FOV) was 250 mm, and the image was reconstructed by using the ICD algorithm [1].

Figs. 1 and 2 show that the proposed methods provide directional weights that lead to more isotropic noise characteristics in reconstructed image. 1D full-width-half-maximum (FWHM) values of the autocorrelation functions along each axis quantitatively verifies the improvements of isotropy of noise property. However, the autocorrelation function does not perfectly match the target. This may be due to under-determined nature of the problem or limited degrees of freedom of our design. Our future works will address this issue with more thorough investigation on the constraints.

Fig. 3 shows the reconstructed images with conventional regularization and proposed regularization. The image reconstructed using the designed directional weights has slightly more uniform noise distribution, which is also illustrated in Table I.

Overall, the proposed method shows potential to obtain more isotropic and uniform noise characteristics for the statistical reconstruction methods.

	Center Slice	End Slice
Conventional	1000 ± 5.22	999 ± 6.85
Designed	1000 ± 5.25	999 ± 5.82

TABLE I

COMPARISON OF IMAGE VALUES IN THE RECONSTRUCTED IMAGES WITH CONVENTIONAL AND DESIGNED REGULARIZERS (UNITS: HU). MEAN AND STANDARD DEVIATION OF IMAGE VALUES WERE CALCULATED FROM 4 CIRCULAR ROIS LOCATED INSIDE THE WATER REGION IN EACH SLICE.

IV. DISCUSSION

We proposed a regularization design method for 3D axial CT that aims to improve uniformity and isotropy of noise characteristics in the reconstructed image. The proposed regularization showed improved noise characteristics compared
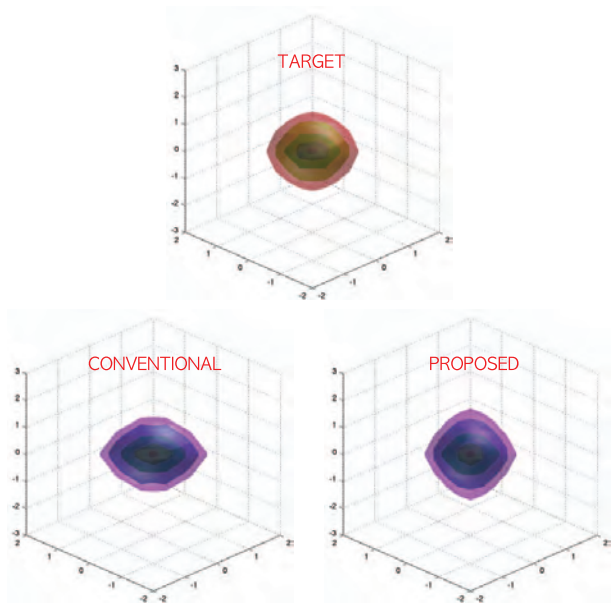

Fig. 1. 3D plots of autocorrelation of conventional regularization (bottom left) and proposed regularization (bottom right) at (60.2,60.2,8.8) (mm). Target autocorrelation is given as a reference (top).
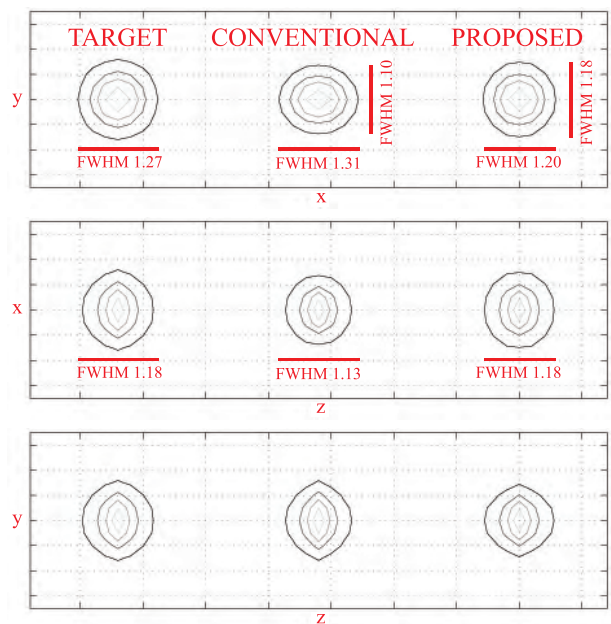

Fig. 2. Autocorrelation of conventional regularization (middle column) and proposed regularization (right column) at (70,0,9.4) (mm). Target autocorrelation is given as a reference (left column). Each row corresponds to xy, xz, and yz profiles, respectively. Each image was normalized with its own peak value.

to the conventional regularization for the full scan geometry. However, the designed impulse responses do not match the target response precisely, and we hope to improve our regularization method with more through investigation. Furthermore, the proposed methods will be verified with more data and other scanning geometries. Since we now have two different regularization design methods aim to improve spatial
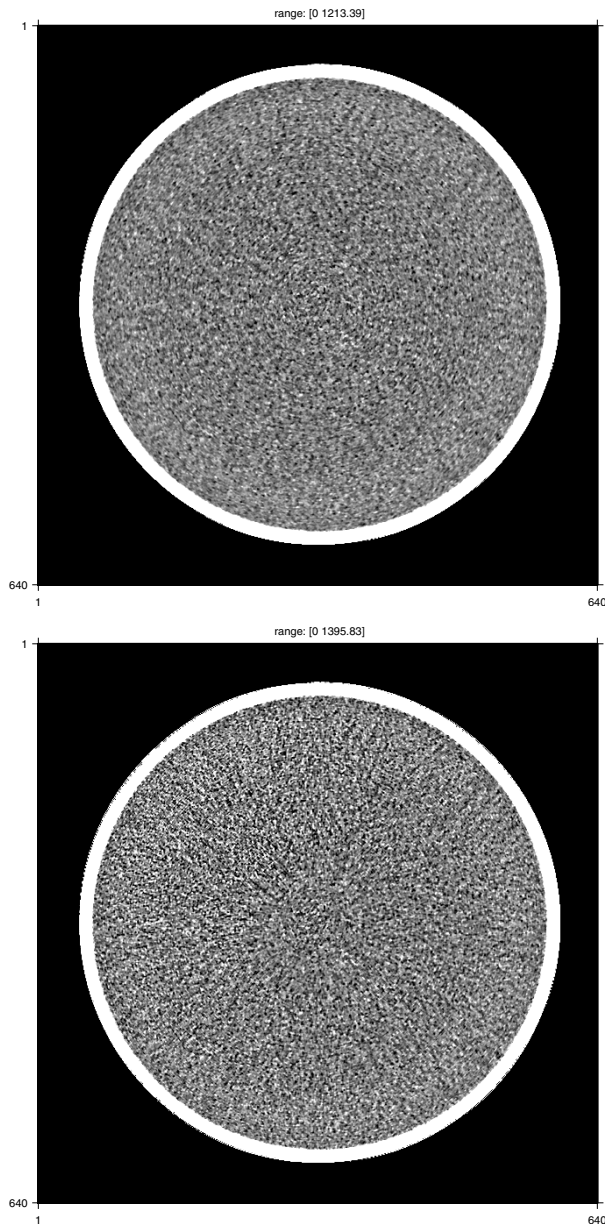
range: [0 1213.39]

range: [0 1395.83]

Fig. 3. Reconstructed images at an end slice using conventional directional weights (top) and designed directional weights (bottom).

resolution and noise characteristics, respectively, we want to compare these two methods to see whether there exists trade-off between these two methods. If possible, combination of two methods will also be investigated.

REFERENCES

[1] J.-B. Thibault, K. Sauer, C. Bouman, and J. Hsieh, "A three-dimensional statistical approach to improved image quality for multi-slice helical CT," *Med. Phys.*, vol. 34, no. 11, pp. 4526–44, Nov. 2007.

[2] J. A. Fessler and W. L. Rogers, "Spatial resolution properties of penalized-likelihood image reconstruction methods: Space-invariant tomographs," *IEEE Trans. Im. Proc.*, vol. 5, no. 9, pp. 1346–58, Sep. 1996.

[3] J. W. Stayman and J. A. Fessler, "Compensation for nonuniform resolution using penalized-likelihood reconstruction in space-variant imaging systems," *IEEE Trans. Med. Imag.*, vol. 23, no. 3, pp. 269–84, Mar. 2004.

[4] H. R. Shi and J. A. Fessler, "Quadratic regularization design for 2D CT," *IEEE Trans. Med. Imag.*, vol. 28, no. 5, pp. 645–56, May 2009.

[5] J. H. Cho and J. A. Fessler, "Quadratic regularization design for 3D axial CT," in *Proc. Intl. Mtg. on Fully 3D Image Recon. in Rad. and Nuc. Med*, 2013, pp. 78–81.

[6] J. A. Fessler, "Mean and variance of implicitly defined biased estimators (such as penalized maximum likelihood): Applications to tomography," *IEEE Trans. Im. Proc.*, vol. 5, no. 3, pp. 493–506, Mar. 1996.

[7] J. Qi and R. M. Leahy, "Resolution and noise properties of MAP reconstruction for fully 3D PET," *IEEE Trans. Med. Imag.*, vol. 19, no. 5, pp. 493–506, May 2000.

[8] S. Schmitt and J. A. Fessler, "Fast variance computation for quadratically penalized iterative reconstruction of 3D axial CT images," in *Proc. IEEE Nuc. Sci. Symp. Med. Im. Conf.*, 2012, pp. 3287–92.

[9] C. L. Lawson and R. J. Hanson, *Solving least squares problems*. Prentice-Hall, 1974.

[10] E. Hansis, D. Schafer, M. Grass, and O. Dossel, "An iterative method for the reconstruction of the coronary arteries from rotational x-ray angiography," in *Proc. SPIE Medical Imaging 2007: Phys. Med. Im.*, 2007.